# STRUCTURAL EVALUATION OF CURVED STIFFENED COMPOSITE PANELS FABRICATED USING A THERM-X$^{sm}$ PROCESS

Christos Kassapoglou    Albert J. DiNicola    Jack C. Chou
Structures Research Section
United Technologies Sikorsky Aircraft
Stratford CT

Jerry W. Deaton
NASA Langley Research Center
Hampton, VA

## INTRODUCTION

The use of composites in aircraft structures is often limited by material and manufacturing costs which, for some designs and applications, are prohibitively high.  To increase the frequency of application of composites in primary airframe components alternative manufacturing processes are sought that reduce cost and/or enhance structural efficiency.

One alternative process involves the use of THERM-X$^{sm}$ as the pressure transfer medium during autoclave curing.  THERM-X$^{sm}$, a silicon- based flowable polymer which behaves like a liquid under autoclave presssure, transmits quasi-hydrostatic pressure to all contacting surfaces of the part to be cured.  Once the autoclave pressure is relieved, THERM-X$^{sm}$ reverts back to the powdery solid state and can be reused many times.

The THERM-X$^{sm}$ process to be evaluated is depicted in Figure 1 and consists of (a) enclosing the tool and part to be cured by a set of frames that create a box, (b) pouring THERM-X$^{sm}$ powder onto the part and filling the box, and (c) placing a vacuum bag over the box assembly.  In this program, a separating non-porous film (Teflon) was placed between the part to be cured and THERM-X$^{sm}$ powder to avoid any contamination.

The use of THERM-X$^{sm}$ has two significant advantages over conventional manufacturing procedures.  First, it eliminates complicated hard tooling since it guarantees uniform pressure transfer and thus good compaction at complex structural details (such as frame-stiffener intersections and corners).  Second, it greatly simplifies vacuum bagging, since once the part to be cured is covered by THERM-X$^{sm}$ powder, the vacuum bag need only conform to a relatively flat shape reducing significantly the number of pleats required.

A program is on-going at Sikorsky Aircraft to evaluate the structural performance of complex composite fuselage structures made with this THERM-X$^{sm}$ process and to quantify the impact of THERM-X$^{sm}$ on manufacturing labor hours and cost.  The program involves fuselage panel  optimization analysis, a building block test program where structural details representative of the full-scale article are analyzed and tested, and static and fatigue test/analysis of the full-scale test articles. The main results of this program are reported in this paper.
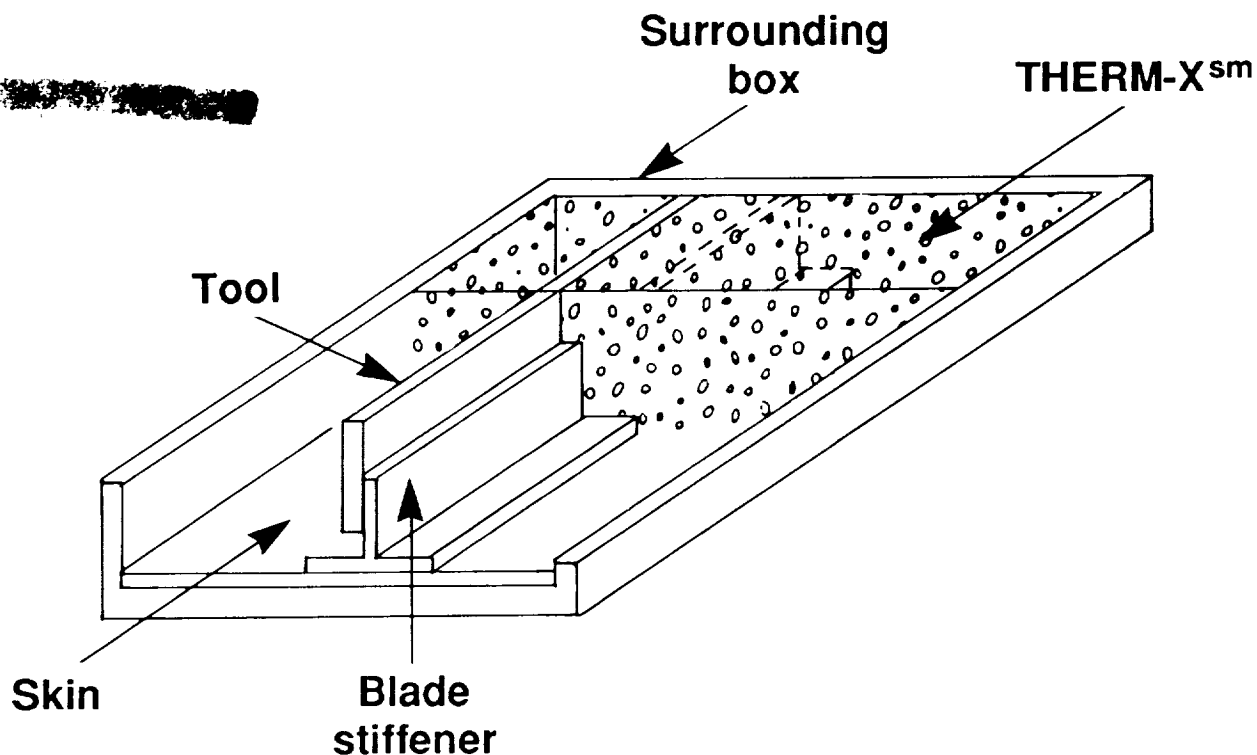
**Surrounding box**

**THERM-X**sm

**Tool**

**Skin**

**Blade stiffener**

Figure 1. Illustration of THERM-X sm Process

## DESIGN SELECTION

An airframe construction representative of both helicopter and fixed wing structure was selected in order to demonstrate the general applicability of the results of this program. Several structural members were evaluated by estimating the impact of using THERM-X sm versus conventional manufacturing. The most common detail with the largest cost savings due to THERM-X sm processing, a curved panel with cocured frames and stiffeners, representing helicopter tailcone and fixed wing fuselage panels, was chosen (see Figure 2). The selection procedure is described in reference 1.

A simple method was developed to optimize the stiffened panel. In this process the skin thickness, frame, and stiffener spacing, and frame and stiffener area and moment of inertia were treated as variables and the weight and cost were minimized subject to loading constraints. The loading constraints were the following: (1) Applied loads were shear and compression (the latter along the stiffeners), (2) Panel failure occurred at a predetermined ultimate load, (3) Buckling of each bay and the panel as a whole occurred at a preselected load combination (fixed postbuckling factor), (4) No material used would be below minimum gage.

Panel failure of the postbuckled panel was determined as first-ply-failure of any of the structural members under the applied loads. A Tsai-Hill stress interaction criterion was used in conjunction with a maximum stress failure criterion. The latter was used to give an idea of the failure mode since, for first ply failure, a transverse tension failure of zero degree plies is very conservative. No such failure mode was noted.
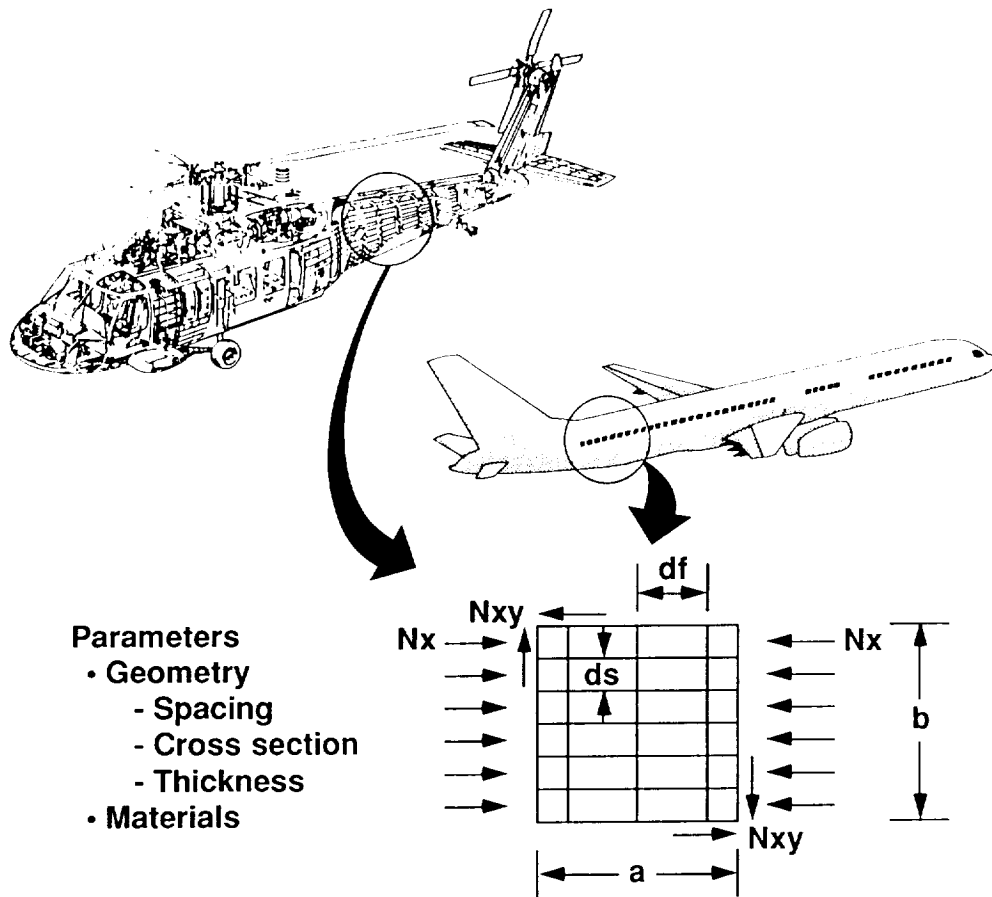
208

**Parameters**
- **Geometry**
  - Spacing
  - Cross section
  - Thickness
- **Materials**

Figure 2.  Stiffened Panel Usage in Aircraft Structures

The cost was a combination of material cost ($50/lb for prepreg material) and labor hours ($30/hr).  Previous Sikorsky experience was used to estimate labor hours required and the effect of increasing stiffener and frame spacing on the total number of manufacturing labor hours.  It was estimated that for each additional stiffener or frame, the manufacturing labor hours for the entire panel would increase by 13% for conventional manufacturing and 8% for THERM-X$^{sm}$ processing.  The 5% difference is due to the reduced bagging complexity of THERM-X$^{sm}$ processing especially around intersecting members such as frames and stiffeners.  For each panel configuration then, the cost was the sum of the raw material cost and the cost to manufacture that particular configuration.  The latter comprised of manufacturing cost for the skin and the cost to fabricate the frames and stiffeners which took into account the 5% cost difference (per added frame or stiffener) between the two manufacturing approaches.  For simplicity in the calculations, the panel was assumed flat and square with 30 inch sides.

The iterative optimization and sizing scheme was applied to various materials and loading configurations.  This process is shown schematically in Figure 3.  The cross-sectional area to spacing ratios for the stiffeners and frames (As/ds and Af/df respectively) are treated as independent parameters.  These ratios are independently selected and the steps outlined in Figure 3 followed until convergence is reached and the panel weight is minimized.  Then, another set of As/ds and Af/df values is selected and the procedure is repeated.  The pair of
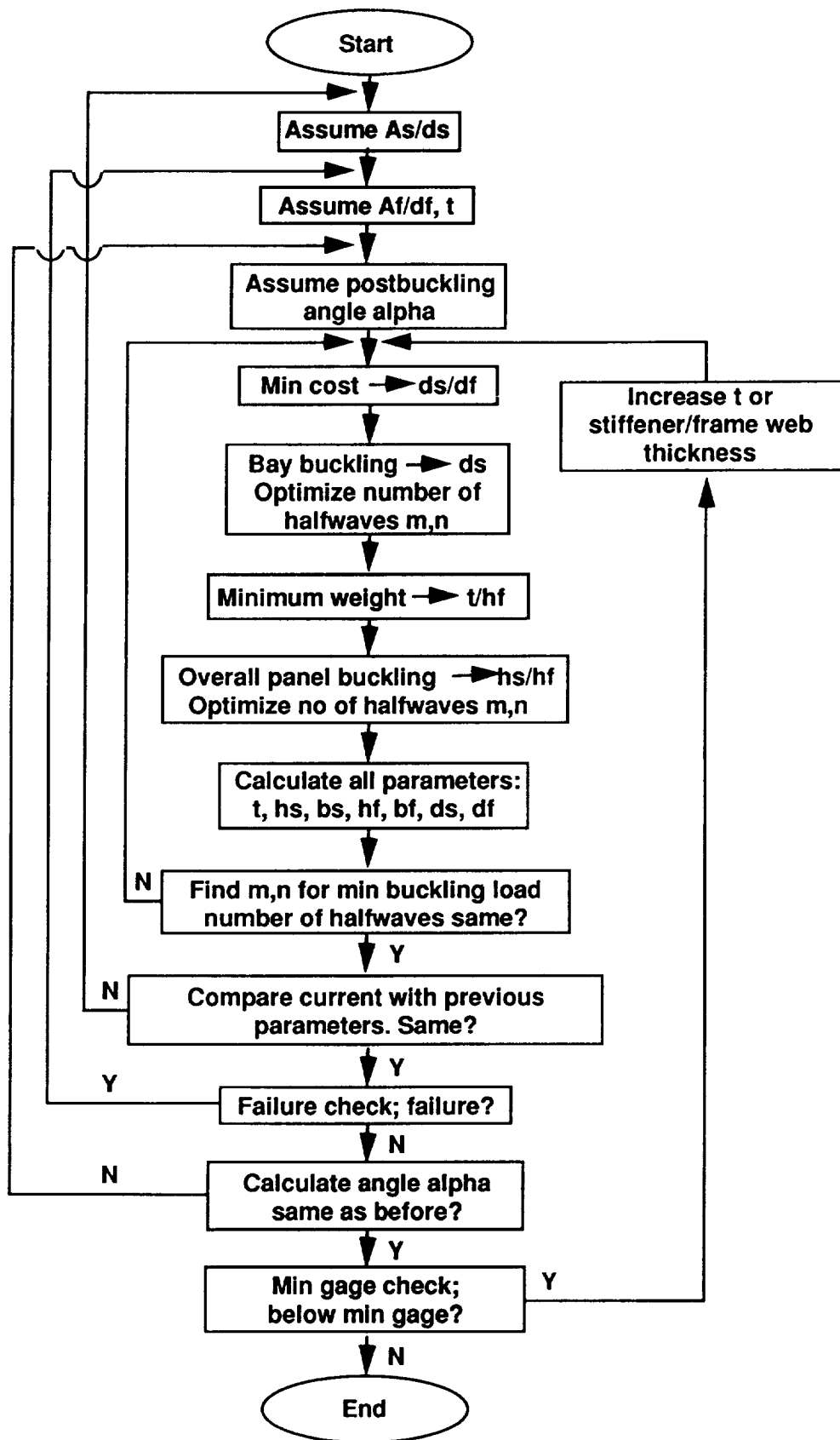
209

Figure 3. Stiffened Panel Optimization Procedure

210

The As/ds and Af/df value finally selected is the one providing minimum weight for all design variations.

A comparison of THERM-X$^{sm}$ processing versus conventional manufacturing for typical helicopter tailcone and fixed wing fuselage loads is shown in Figures 4 and 5. For the helicopter tailcone configuration the ultimate loading design requirement was 250 lb/inch in compression and 250 lb/inch in shear (selected based on S-76 tailcone ultimate design loading). For the fixed wing configuration the ultimate loading was 2500 lb/inch in compression and 1250 lb/inch in shear corresponding to typical fuselage loads [2].

The (normalized) cost to manufacture stiffened panels for typical helicopter tailcones as a function of stiffener spacing ds is shown in Figure 4. The frame spacing df is determined by the optimization procedure (cost minimization equation) to be very nearly equal to 3.2 ds. Two cost curves are shown, one for standard manufacturing and one for THERM-X$^{sm}$ processing. For each geometry configuration, the cost is calculated as the raw material cost plus labor hours to manufacture based on previous Sikorsky Aircraft experience. It is important to note that the minimum cost configuration involves few frames and stiffeners (ds = 5 in.) of large area and moment of inertia and with thick skin, thus corresponding to a relatively high weight. For the loading considered here, the minimum weight configuration would be a minimum gage configuration (with minimum gage thickness for frame and stiffener webs) corresponding to a stiffener spacing less than 1 inch. Thus, the lightest configuration is labor intensive because it involves many stiffeners.

A tradeoff between weight and cost can then be established. At small stiffener spacings the panel weight is low but the manufacturing cost is high. At high stiffener spacings the cost is low but the panel weight is high. An equilibrium between the two driving quantities (weight and cost) can be found by considering the premium in dollars per pound (termed value of improved performance in Figure 4) the customer is willing to pay to reduce the structural weight by one lb. For example, for UH-60 (BLACKHAWK) helicopters, that value is $750/lb.

In this context, since the minimum weight (still meeting the loading requirements) is that corresponding to a minimum gage design, any other acceptable configuration will have a potential weight penalty equal to the difference in weight from the minimum gage configuration. By multiplying this weight difference by the weight premium dollar value (termed here value of improved performance), an upward sloping curve (with increasing ds) is obtained that shows the weight penalty for each configuration translated to dollars. Various curves corresponding to different values of improved performance are shown in Figure 4.

The points of intersection of the weight penalty curves with the cost curves define optimum points, each corresponding to a different selection of manufacturing process and dollar value of improved performance. Any configuration away from the intersection points implies that for the particular manufacturing method selected, either the weight or the cost of the panel can be reduced and still meet the load requirements and the selected value of improved performance.
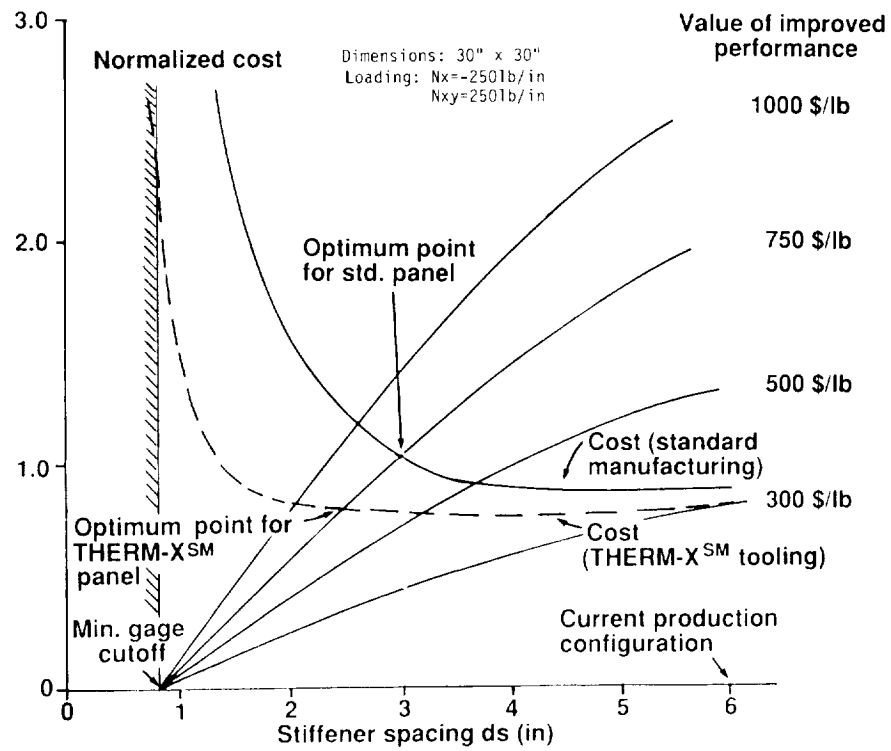
Figure 4.   Determination of Optimum Geometry for Stiffened Panels in Helicopter Structures
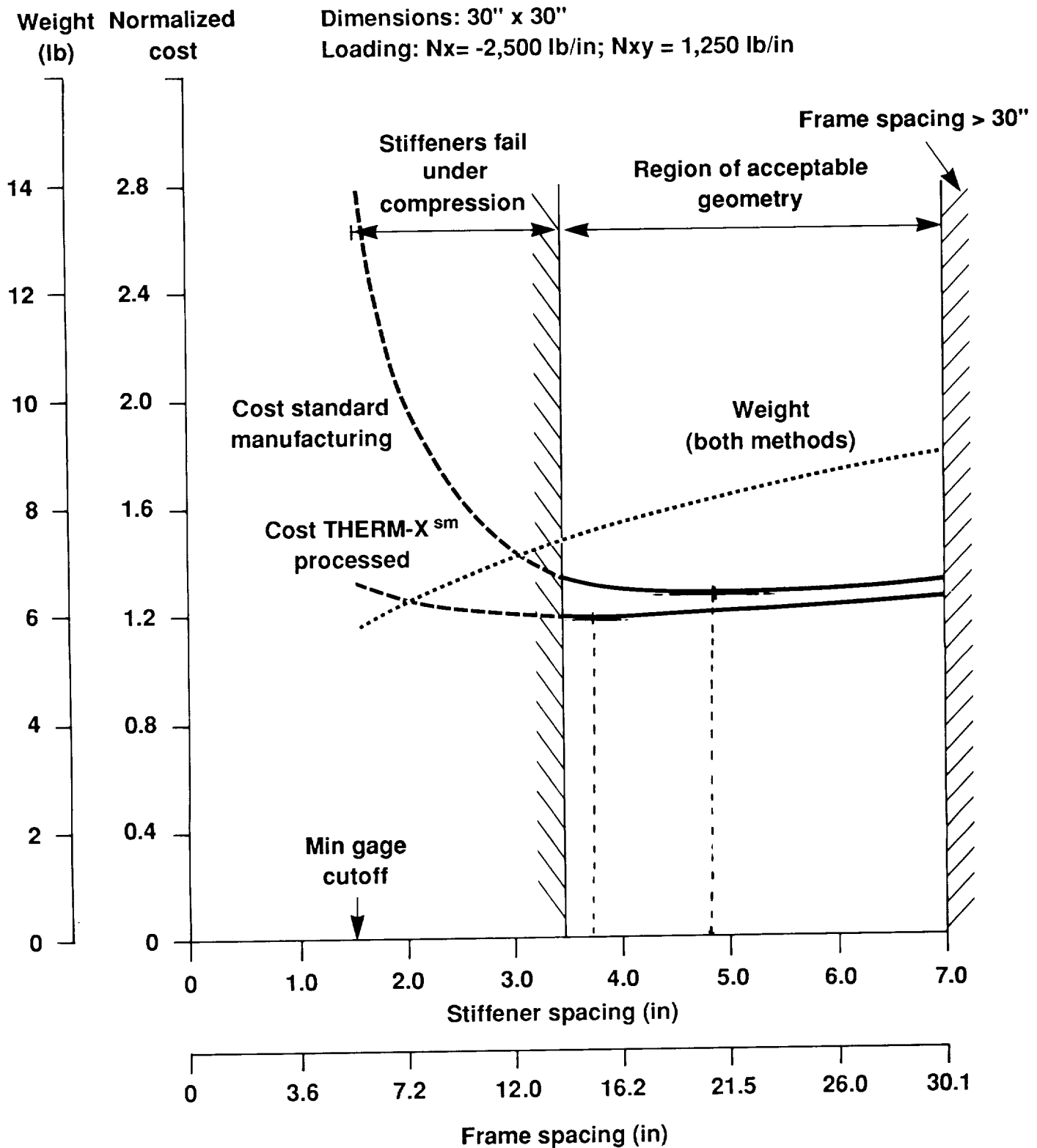
# STIFFENED PANEL OPTIMIZATION



Figure 5. Determination of Optimum Geometry for Stiffened Panels in Fixed Wing Structures

The configuration selected for the full-scale article corresponds to a stiffener spacing of 6.5 inches. This corresponds to a value of improved performance of $300/lb which was felt to be more representative of commercial fixed wing transport. At that spacing the THERM-X$^{sm}$ process results in panels approximately 10% less expensive than conventionally manufactured panels. At smaller stiffener spacings (for higher values of improved performance) the savings can be as high as 22% (ds= 3 inches). It should be noted that these savings do not include savings in tooling. The THERM-X$^{sm}$ process requires relatively simple tooling even for complex parts with cocured frames and stiffeners.

The effect of applied loading can be seen if Figure 4 is compared to Figure 5. In Figure 5, the optimization process was applied to panels with loadings representative of fixed wing transport fuselages. In this case, the minimum gage configuration is not attainable since the loading is high. The limiting factor at low stiffener spacings is the compression failure strength of the hat stiffeners assumed in this case to be 36000 psi which corresponds to the first ply failure load of a predominantly 45 degree stiffener web layup. This is shown by the left vertical curve at ds=3.5 inches.

Two cost curves are shown in Figure 5 much like the ones in Figure 4. In this case however, the weight change between the minimum weight configuration (at ds = 3.5 in.) and any other acceptable configuration is so small that the value of improved performance should be higher than $10000/lb for the weight penalty curves to intersect the cost curves. For that reason, the weight penalty curves are not included. Instead, to show the tradeoff between cost and weight, the minimum weight of the panel for each value of stiffener spacing is shown as an upward sloping curve. The corresponding frame spacings are also shown in Figure 5.

Figure 5 suggests that the minimum weight configuration corresponds to ds=3.5 inches while the minimum cost configuration corresponds to ds=3.75 inches for THERM-X$^{sm}$ processed panels and 4.75 inches for conventionally manufactured panels. The user will then have to make a choice on which configuration to select favoring either a minimum weight or a minimum cost design.

The conclusions can change significantly if the compression strength of the hat stiffeners is increased. That would move the left cutoff line to the left increasing the number of acceptable configurations. This would also increase the savings of the THERM-X$^{sm}$ processed panels from approximately 6% (at ds=5 inches for example) to over 15% (at ds=3.0 inches).

As a final comment on the optimization study, the current approach does predict that the commonly used configuration of ds=6 inches and df=20 inches in aircraft structures is one of the acceptable configurations but corresponds to a higher weight configuration than can be attained with lower ds values. It should be borne in mind that the current process assumes a flat panel and neglects the stiffening effect afforded by curved panels. This effect would yield optimum configurations with ds values higher than currently predicted, thus closer to the commonly used value of ds=6 inches.

The configuration selected based on the optimization process (ds=6.5 inches, df=20 inches, Nx=-250 lb/in, and Nxy=250 lb/in at ultimate) was evaluated with a detailed test and analysis program that is described in the next section.

214

A representative sketch of the curved and stiffened composite panel under consideration is shown in Figure 6. In order to provide a basis for verification of predicting failure modes and the panel's ultimate load, the six building block tests also shown in the figure were performed prior to full-scale testing. Detailed results of these building block tests were reported previously [1]. Comparable, and often enhanced, strength and stiffness values were noted for THERM-X$^{sm}$ processed test specimens versus those conventionally manufactured, and excellent laminate quality control was attainable with substantially less effort. A summary of the data generated during the tests, which will verify analysis and assist in predicting ultimate load for the full-scale test, is presented in Figure 7.

Compression after impact tests were performed for the two damage regimes envisioned for the composite fuselage panel: low speed-high mass impact and high speed-low mass impact. The former is representative of "tool drop" style impact damage and the latter is characteristic of in-flight impact damage. Shear after impact tests were performed under low speed conditions only [1] since the trends of high versus low speed impact established for the compression specimens are expected to apply in this instance.
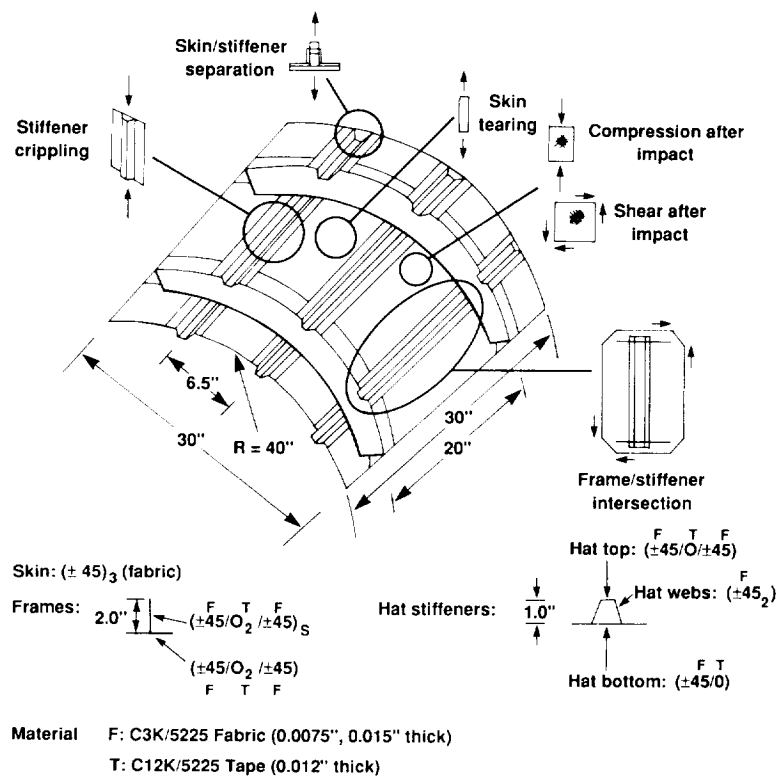


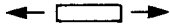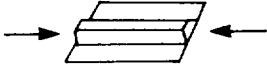Figure 6. Building Block Approach and Full-Scale Article Configuration
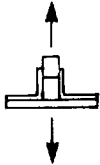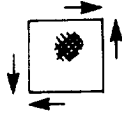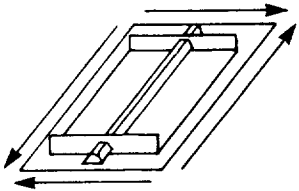
| Building Block Evaluation | Configuration | Number Specimens | Results |
|---|---|---|---|
| Skin tearing | ← ▭ → | 8 | Tensile modulus: 10 MSI<br>Tensile strength: 99 KSI |
| Stiffener crippling | → ◢ ← | 6 | Crippling strength:<br>14,628 PSI |
| Skin/stiffener separation | ↕ | 5 | Pull-off strength:<br>90.5 lb/in |
| Compression after impact | → ▣ ← | 10 | Residual strenght vs impact energy and indentation at point of impact for high and low speed impact (See fig. 8-10) |
| Shear after impact | ▣ | 5 | |
| Frame-stiffener intersection | | 3 | Failure load at the intersection of the frame and  Hat stiffener :<br>614 lb/in |

Figure 7.  Summary of Building Block Approach Results

216

A summary of the average normalized compression after impact (CAI) strength values is presented in Figure 8 for both velocity regimes and fabrication procedures. Conventional manufacturing appears to provide moderately superior CAI strength at both 600 and 1200 in-lb/in impact energies (15% and 3.3% respectively). The slight advantage afforded by conventional manufacturing was noted for both impact velocities. The underlying reason for the strength discrepancy is currently being investigated. The only significant difference between the two manufacturing methods, which may account for the residual strength discrepancy, is that the cure pressure for THERM-X$^{sm}$ processing is twice that used during conventional manufacture (100 psi versus 50 psi). More tests are needed to quantify these differences with statistical significance.

Internal damage resulting from impact as measured by ultrasonic C-scan is shown in Figure 9 for both fabrication procedures and velocity regimes. Consistent with other literature citations [for example references 3 and 4], the high speed impact event produced greater levels of internal damage than low speed impact for a fixed energy level. For 600 in-lb/in of impact energy, THERM-X$^{sm}$ processed specimens exhibited greater internal damage area (by 21%) whereas at 1200 in-lb/in of energy both fabrication procedures yielded similar amounts of internal damage.

There is evidence that indentation at the point of impact is an effective means to correlate a measureable quantity to resultant post-impact strength [1]. A comparison of average indentation for conventionally manufactured and THERM-X$^{sm}$ processed specimens is shown in Figure 10. Although indentation data for high speed impact of THERM-X$^{sm}$ panels were not available, the consistency of the data at hand indicates, irrespective of either velocity regime or manufacturing procedure, indentation may be a reliable way to predict resultant strength after impact.
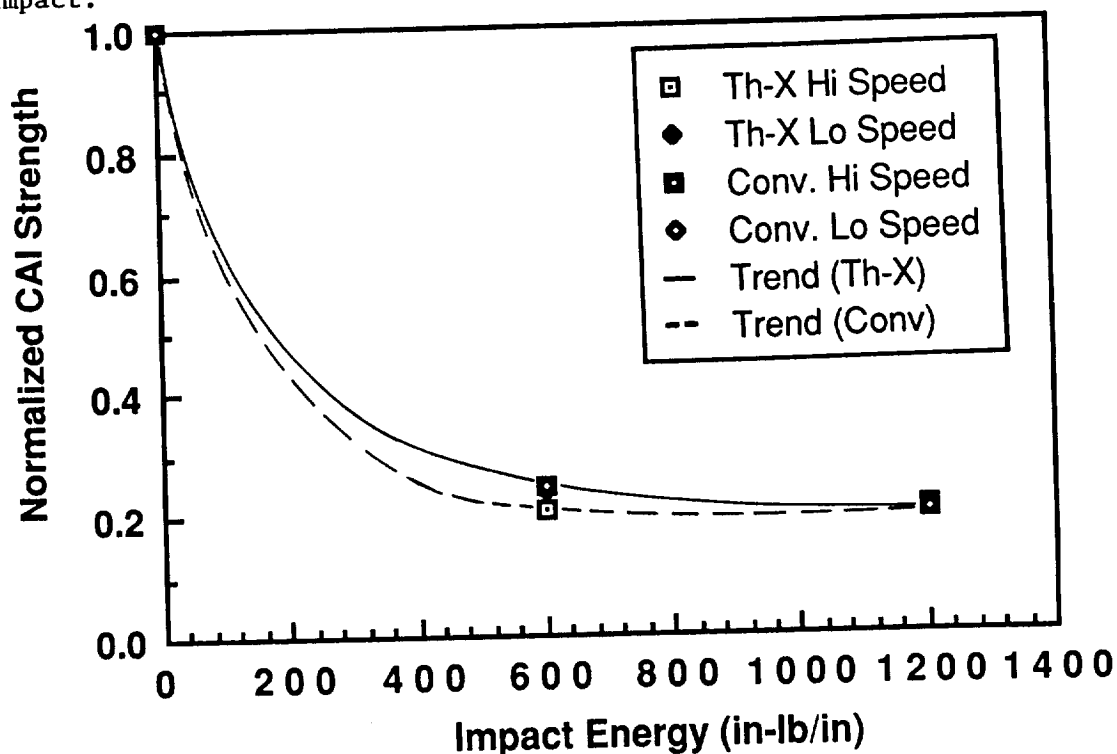


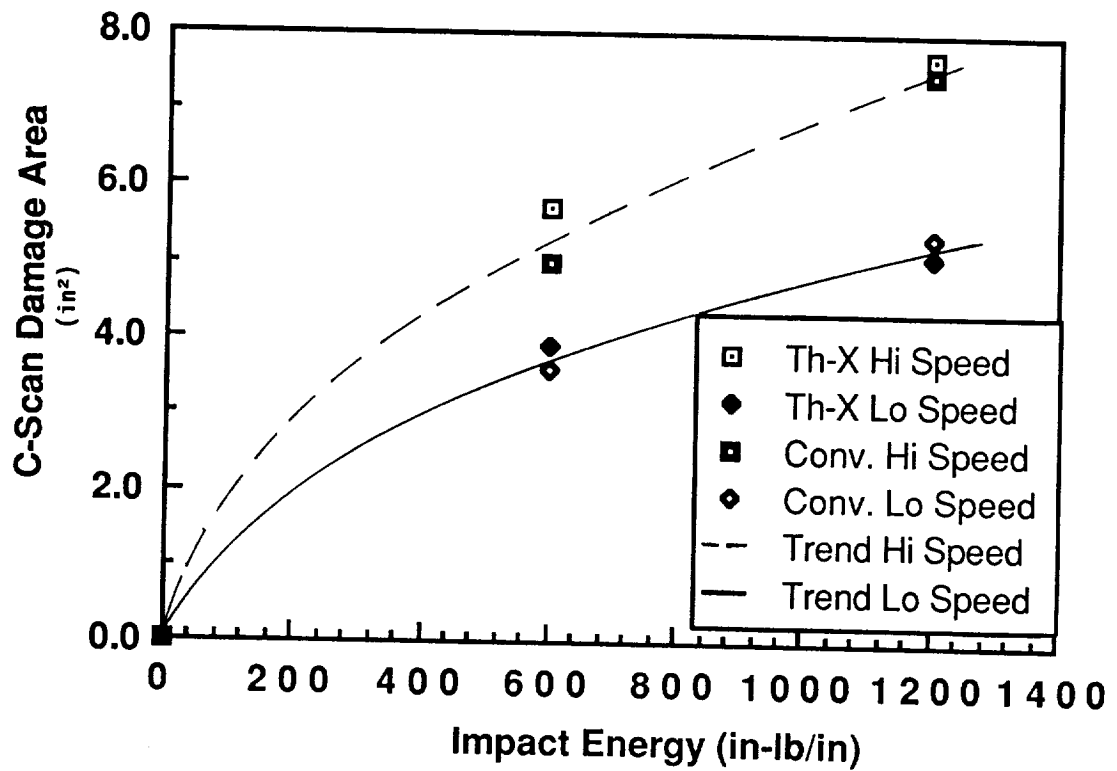Figure 8. Compression after Impact Strength as a Function of Impact Energy

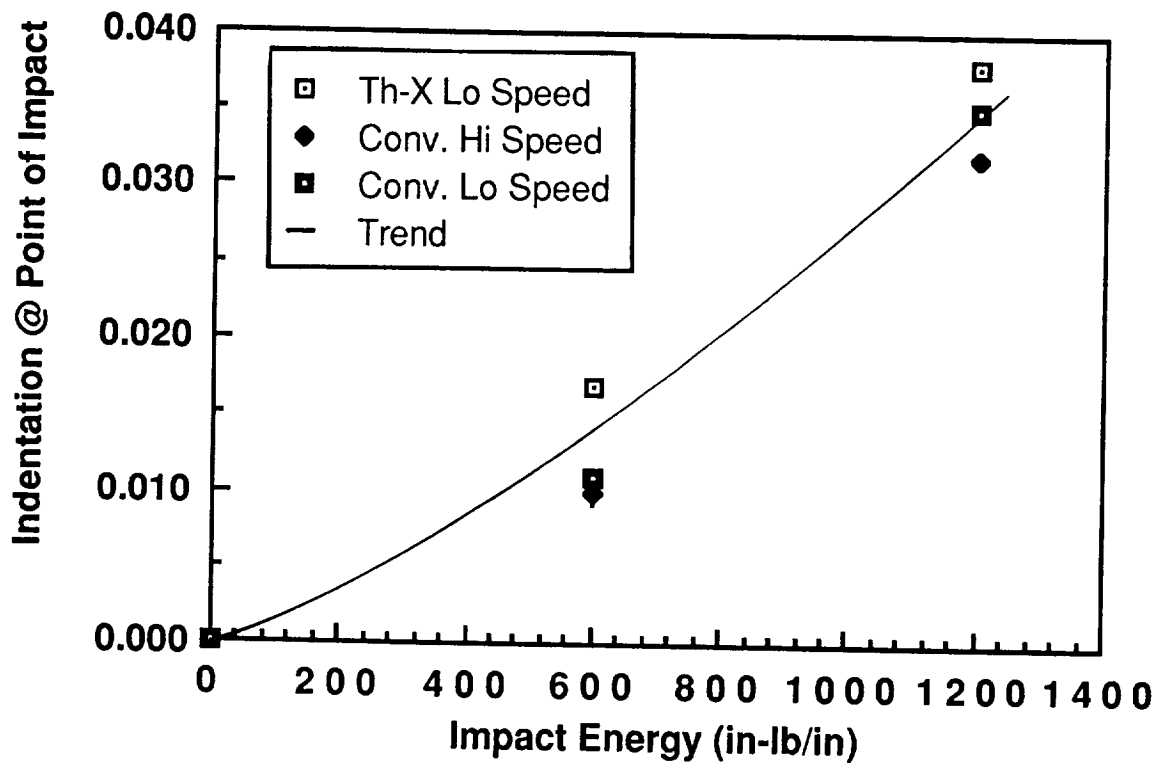Figure 9.  Variation of C-Scan Indicated Damage Area with Impact Energy



Figure 10.  Indentation at Point of Impact as a Function of Impact Energy

218

## Flat Frame/Stiffener Intersection Specimen

The frame-stiffener intersection specimen is used to provide experimental evaluation of failure mechanisms present in the full-scale article at the intersecting corners of frames and stiffeners, a link between flat and curved specimens, and to support corresponding analysis predictions.

The specimen is shown in Figure 11. It represents two bays of the full-scale curved stiffened panel. A closeup of a typical frame/stiffener intersection corner is shown in Figure 12. Excellent consolidation and radius definition is evident. Part quality around the shear tie which consists of the outer plies of the frame web cocured on the hat stiffener webs is also very high with accurate placement and contour definition. The layup of the skin, frames and stiffeners is identical to that of the full scale article as shown in Figure 6. Aluminum doublers 0.5 in. thick and 3.0 in. wide were used for load introduction fastened on three-ply graphite/epoxy doublers that were cocured with the specimen. The aluminum doublers formed a picture frame fixture for testing the specimens in shear.

The finite element model used is shown in Figure 13. One specimen end is loaded in tension (along a diagonal) and the opposite end is fixed. MSC NASTRAN SOL 66 geometric nonlinear solution was used to determine the buckling load and post buckling behavior of the panel. The model consists of 606 grid points, 576 CQUAD elements, and 3601 degrees of freedom.

## Comparison of Test Results to Finite Element Predictions

The strain gage data obtained from the frame-stiffener intersection specimens was compensated for gage transverse sensitivity and percent reinforcement (resulting from gage bagging and adhesive material) following procedures recommended by the gage manufacturer (Micro-Measurements Division, Measurement Group Inc., Raleigh NC) and reference 5.

For the type of gages used (CEA-03-063UR-350) the transverse gage sensitivity is insignificant (only 1% change to the apparent strain). The percent reinforcement effect however, for the materials and layups used, ranges from 0.6% to 15.8% (depending on the gage installation such as back-to-back or single face, laminate thickness, and open face versus encapsulated gage configuration). The results reported below have this correction included wherever it is considered significant (more than 5%).

The strain gage locations (total of 18 rosettes) were chosen to give a detailed strain distribution throughout the specimen and in particular at skin bays and near the frame-stiffener intersections. Finite element predicted surface strains are compared to test results at various panel locations and load levels in Figures 14 through 17. The locations are (1) Hat Stiffener Center (Figure 14), (2) Frame-Stiffener Intersection Corner (Figure 15), (3) Bay Quarter Point (Figure 16), and (4) Bay Center (Figure 17). At low applied loads (except for the frame-stiffener intersection location) and high loads close to the failure load (in all cases), the finite element predictions are in very good agreement with the experimental results. At intermediate loads the correlation ranges from poor (bay center and frame stiffener intersection corner) to excellent (hat stiffener center and bay quarter point).
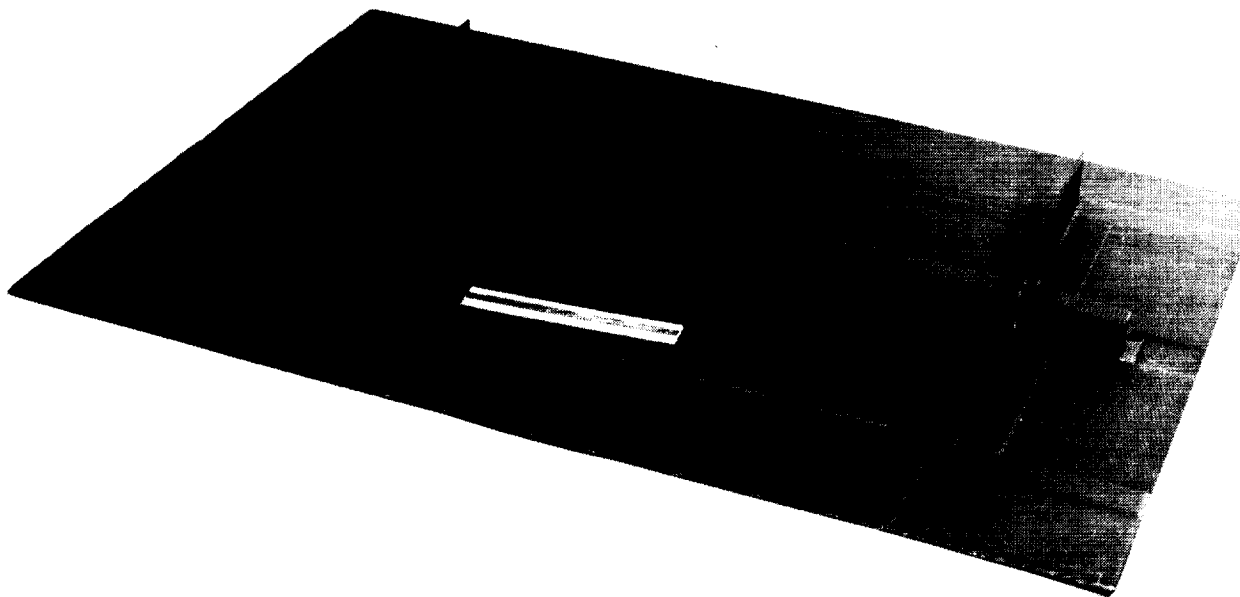
Figure 11. Flat Frame/Stiffener Intersection Specimen (Stiffened Side Overview)
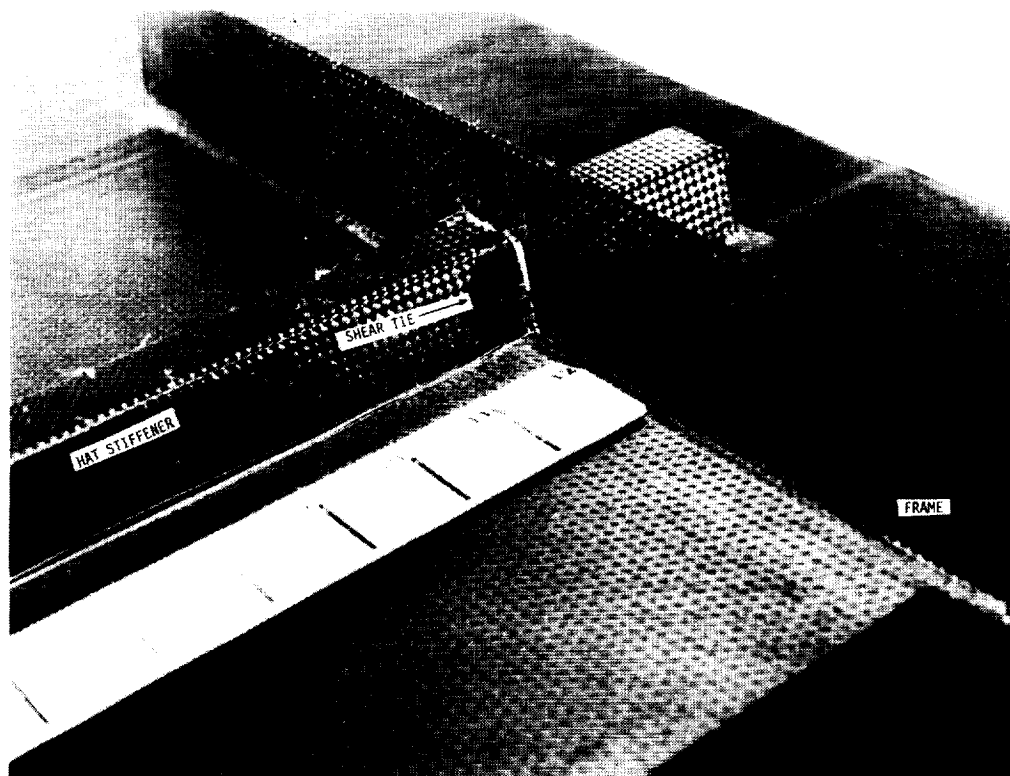


Figure 12. Frame-Stiffener Intersection Detail

The shadow moire method was used to monitor the out-of-plane displacements of the panel during the test. The first moire fringe pattern appeared at an applied load of 2600 lbs and is shown in Figure 18. The postbuckling mode shape just before the panel failure load of 20000 lbs is shown in Figure 19. The analysis of the photographs of the moire fringe pattern follows standard procedures outlined in the literature [6].

Typical experimental and analytical results for the out-of-plane displacement along the panel skin bay at the applied load of 16000 lbs is shown in Figure 20. The moire measured amplitude correlates well with the finite element prediction. However, the wavelength of the deflection mode shape is less than the finite element prediction. The discrepancy between finite elements and moire pattern data is attributed to local eccentricities of the specimen and resulting differences in load transfer.

The failure prediction for these specimens was obtained by determining the most highly loaded element in the finite element model and using the forces and moments on that element as input in a first ply failure criterion. That element coincided with the location where a crack initiated (near the bay corner) during testing. Using mean material allowables the failure prediction using a stress interaction criterion [7] is 26000 lbs of applied load. The corresponding B-Basis prediction is 22950 lbs. The test failure load (average of two specimens) is 21000 lbs (614 lbs/in). The failure predictions are based on allowables for conventionally manufactured parts and are off by 9 to 24% (B-Basis versus mean allowable predictions). There are two reasons for the discrepancy: (1) Loading of the first test specimen was stopped when the first
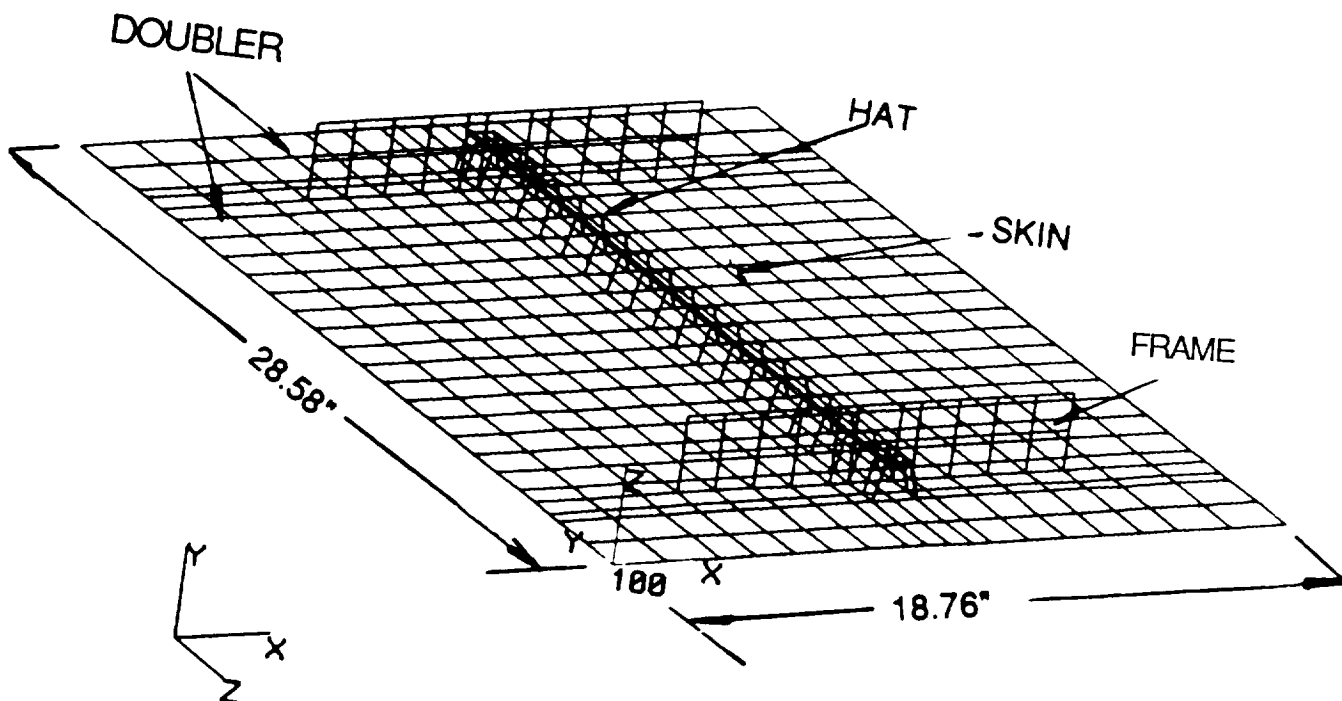


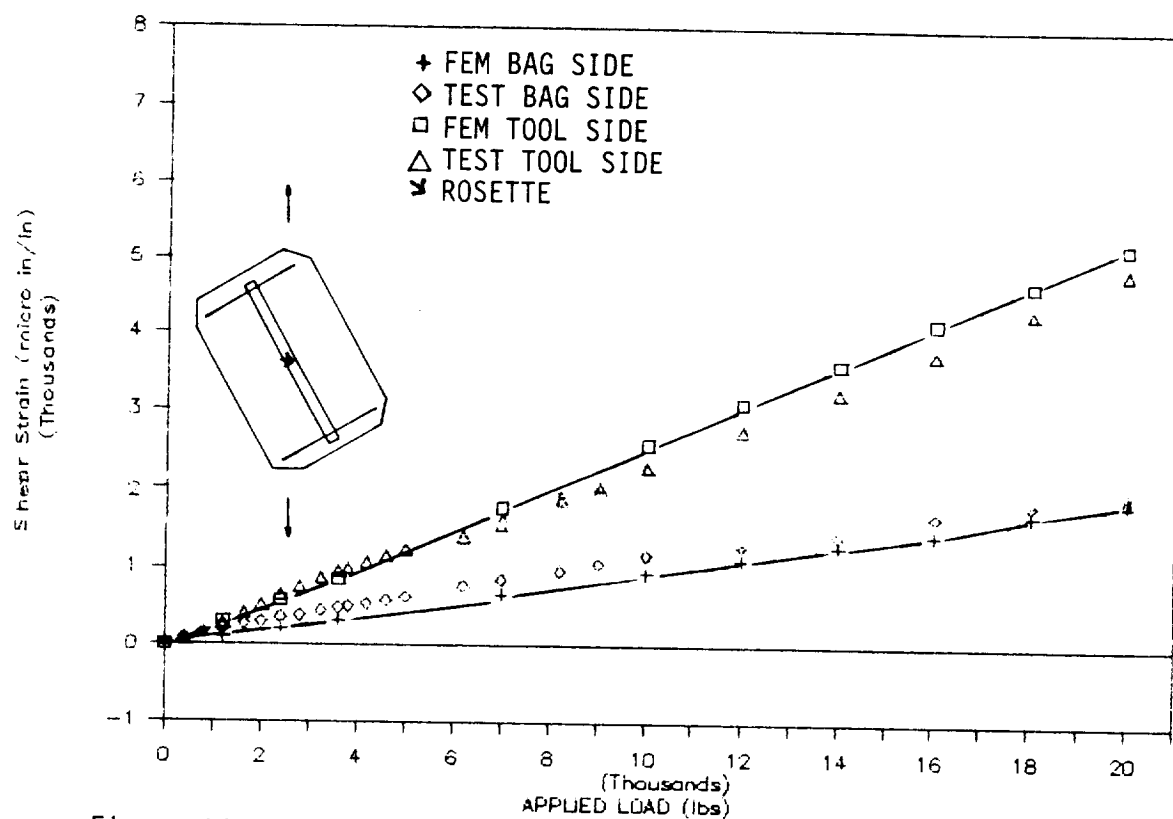Figure 13. Finite Element Mesh for Frame/Stiffener Intersection
Specimen

Figure 14. Comparison of Finite Element Predictions to Test Results at Hat-Stiffener Center (Shear Strains - Intersection Specimen)
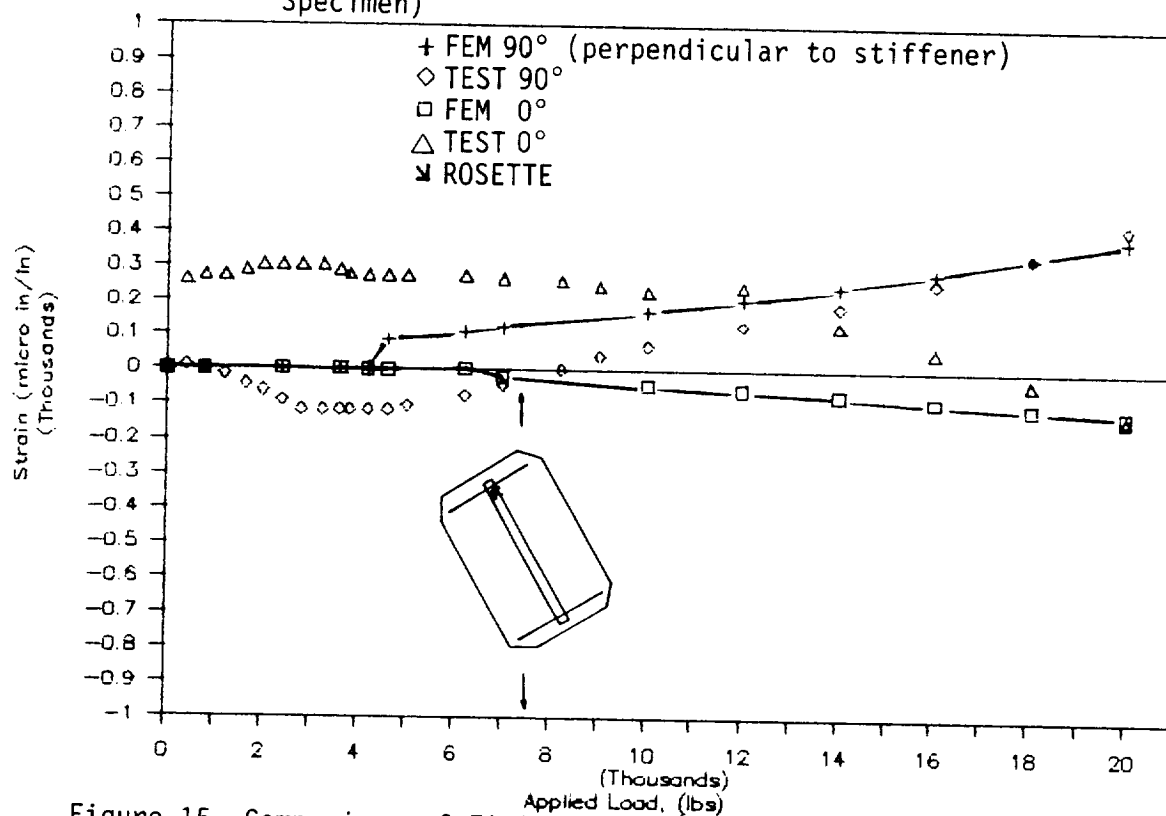


Figure 15. Comparison of Finite Element Predictions to Test Results at Frame/Stiffener Intersection Corner
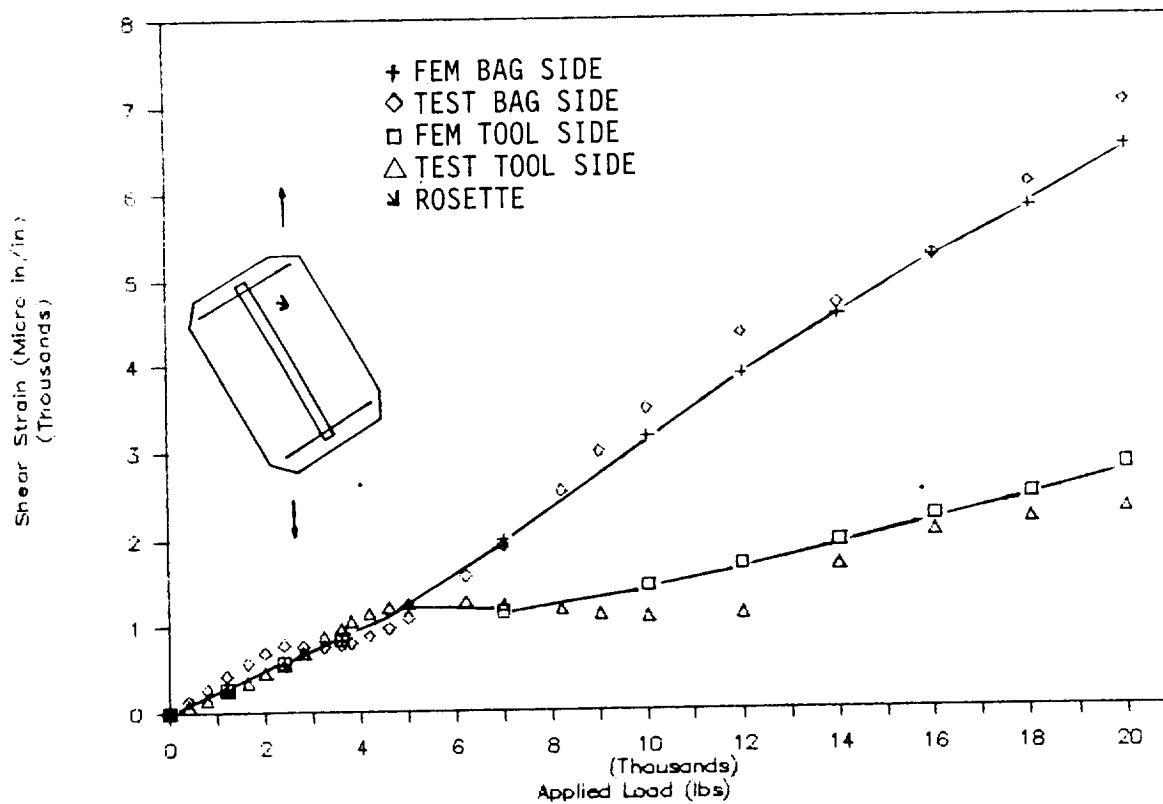
222

Figure 16. Comparison of Finite Element Predictions to Test Results at Bay Quarter Point (Shear Strains - Intersection Specimen)
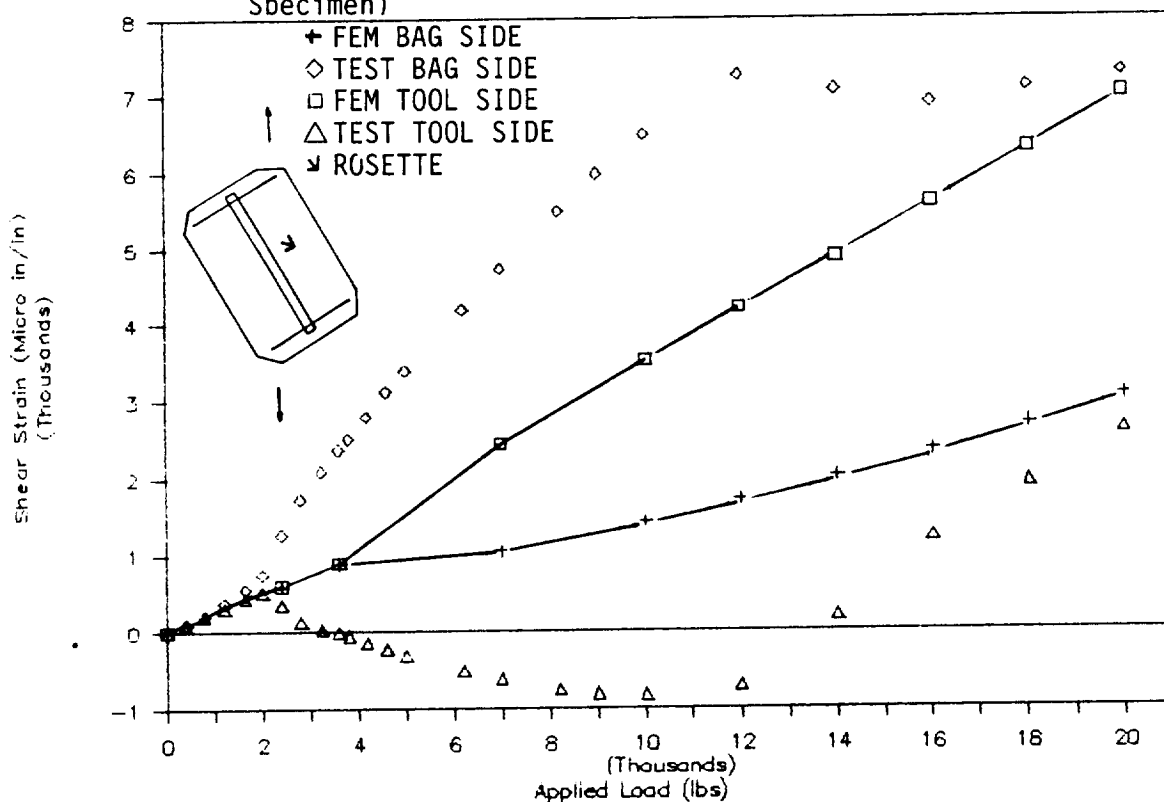


Figure 17. Comparison of Finite Element Predictions to Test Results at Bay Center (Shear Strains - Intersection Specimen)
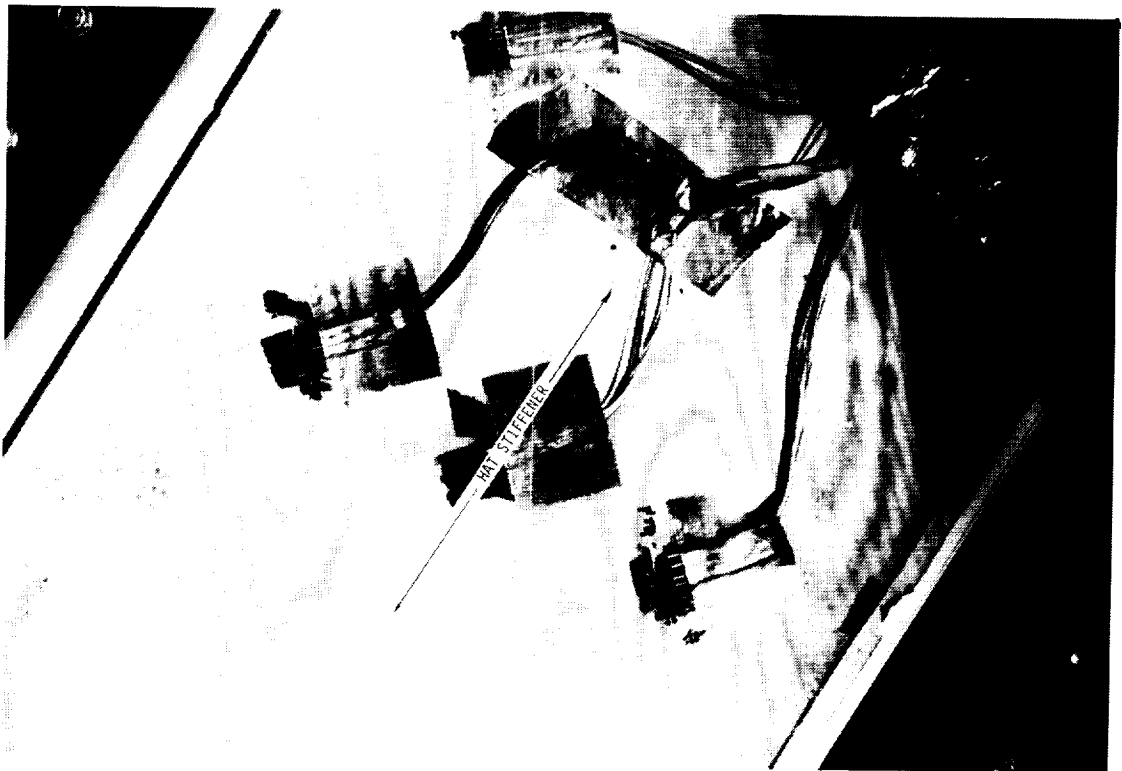
223

Figure 18. First Shadow Moire Fringes on Frame/Stiffener
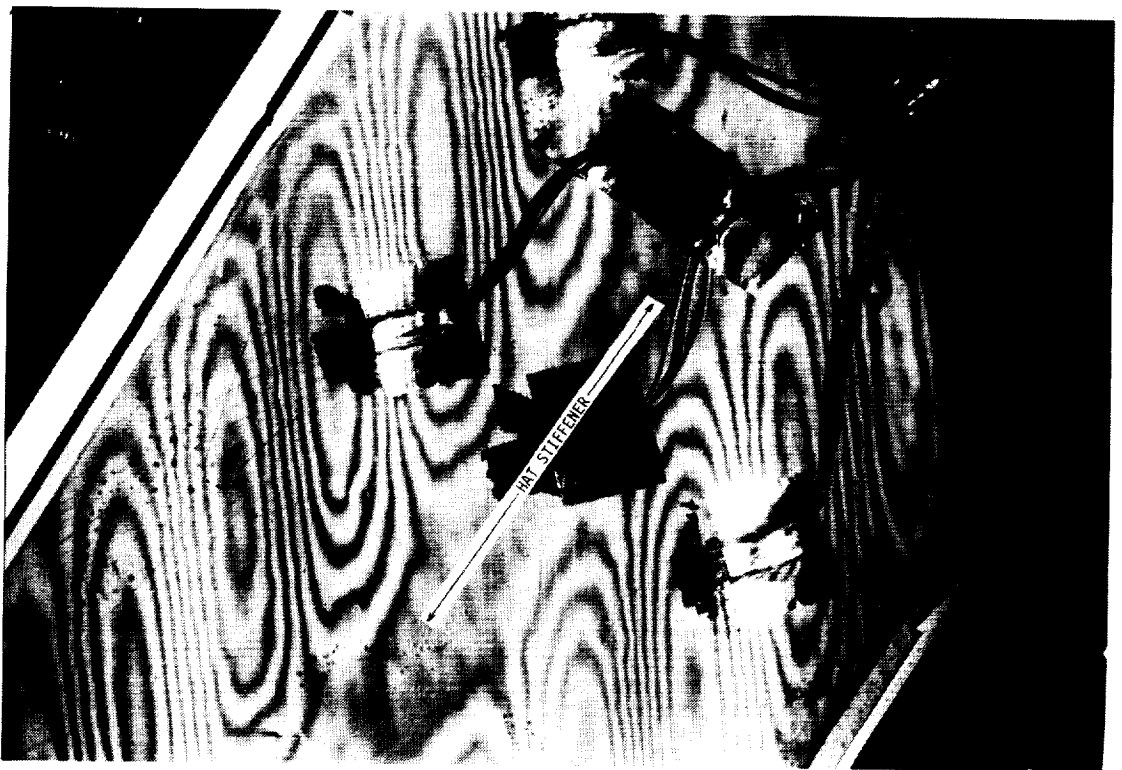Intersection Specimen (2600 lbs)



Figure 19. Shadow Moire Fringes Near Failure of Frame/Stiffener
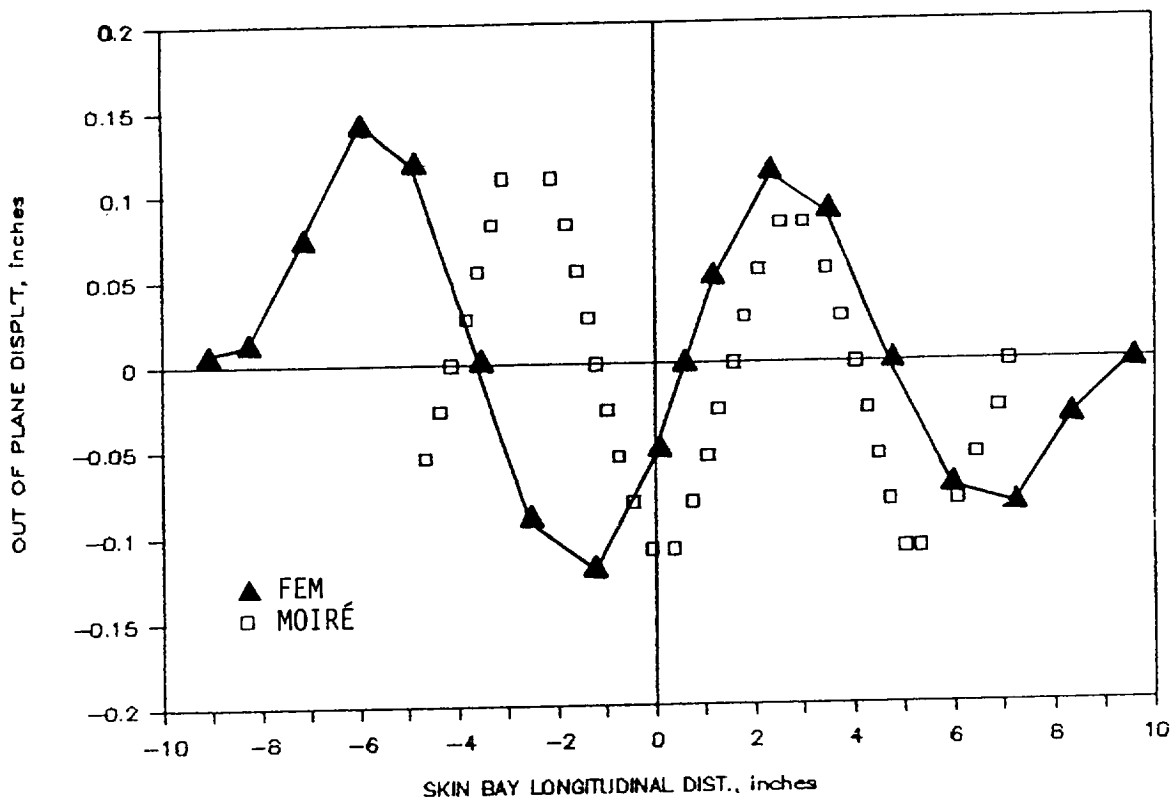Intersection Specimen (20000 lbs)

224

Figure 20. Comparison of Out-of-Plane Deflection Shape at Bay Center Along Stiffener Axis

cracks developed (at 20000 lbs) in order to see where failure started. The load capability may have been significantly higher as is indicated by the failure load for the second specimen (22000 lbs). Thus, the average test failure load of 21000 lbs may be conservative. (2) Based on post-test examination, final failure was determined not to result from corner cracking (that was noted in the specimen) but rather from high local strains in the vicinity of the root of the hat stiffener (near the frame/stiffener intersection) due to the buckled shape. This is verified by the shadow moire fringes (Figure 19), which do not cross the centerline of the specimen but stop where the stiffener webs meet the skin. The fringes, which indicate out-of-plane deflection, tend to come close together in the vicinity of the stiffener. This implies a large displacement gradient is present in this area and the associated high bending moments precipitated final failure. The existence and location of this high strain area was confirmed by the finite element analysis.

## FULL-SCALE ARTICLE

The full-scale article (shown in Figure 6) was manufactured by laying up the skin in an aluminum tool that was surrounded by an aluminum frame similar to that shown in Figure 1. The hat stiffeners were laid up around teflon mandrels and placed in position on the skin. The frames were laid up on a specially made tool and then lowered into place in the assembly. Two aluminum cross members, one for each frame, were used to keep the frames in place during curing, in a manner similar to the tool shown in Figure 1. The outer web plies of the frames opened up to accommodate the hat stiffeners going through and
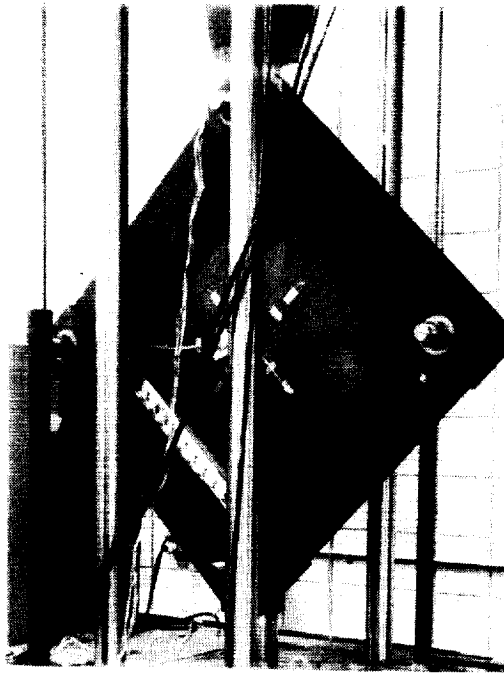
225

Figure 21. Full-Scale Test Setup

served as shear ties between frames and stiffeners. The top skin ply was placed last, covering all stiffener and frame flanges (embedded flange concept). The full-scale panel was tested in shear using a picture frame fixture (Figure 21). Axial load was applied to diagonally opposite ends of the fixture in order to introduce the desired shear loads through the structure. The finite element modelling procedures were the same as for the frame-stiffener intersection specimens. The model had 2530 nodes and 7590 degrees of freedom with 2424 CQUAD4 and 136 CBEAM elements.

A comparison of strain gage data near a frame/stiffener intersection (corner of outer bay) to finite element predictions is shown in Figure 22. The shear strain at a point inside one of the bays (quarter of the distance between the two hat stiffeners) is shown in Figure 23. The axial strain along the frame axis at the center of one of the outer bays is shown in Figure 24. In all cases, test and finite element analysis are in good agreement up to 10000 to 12000 lbs of applied load (postbuckling factor of about 3). The differences at higher loads are due to local failures that occurred (manifesting themselves with loud noises and sharp increases in the deflection gage measurements) and redistributed the load. These local failures were not modelled by the finite element model. The deflection pattern over the whole panel was monitored by shadow moire. In addition, a deflection gage positioned at the center of one of the two center bays was used to measure deflection locally. The out-of-plane deflection at that location is compared to the finite element predictions in Figure 25. For the same load, the deflections predicted by finite elements are 20-30% less than test results through panel failure.

Figure 25 shows that the bay buckling load predicted by finite elements is in excellent agreement with the test result of 4000 lbs (94 lbs/in). A more
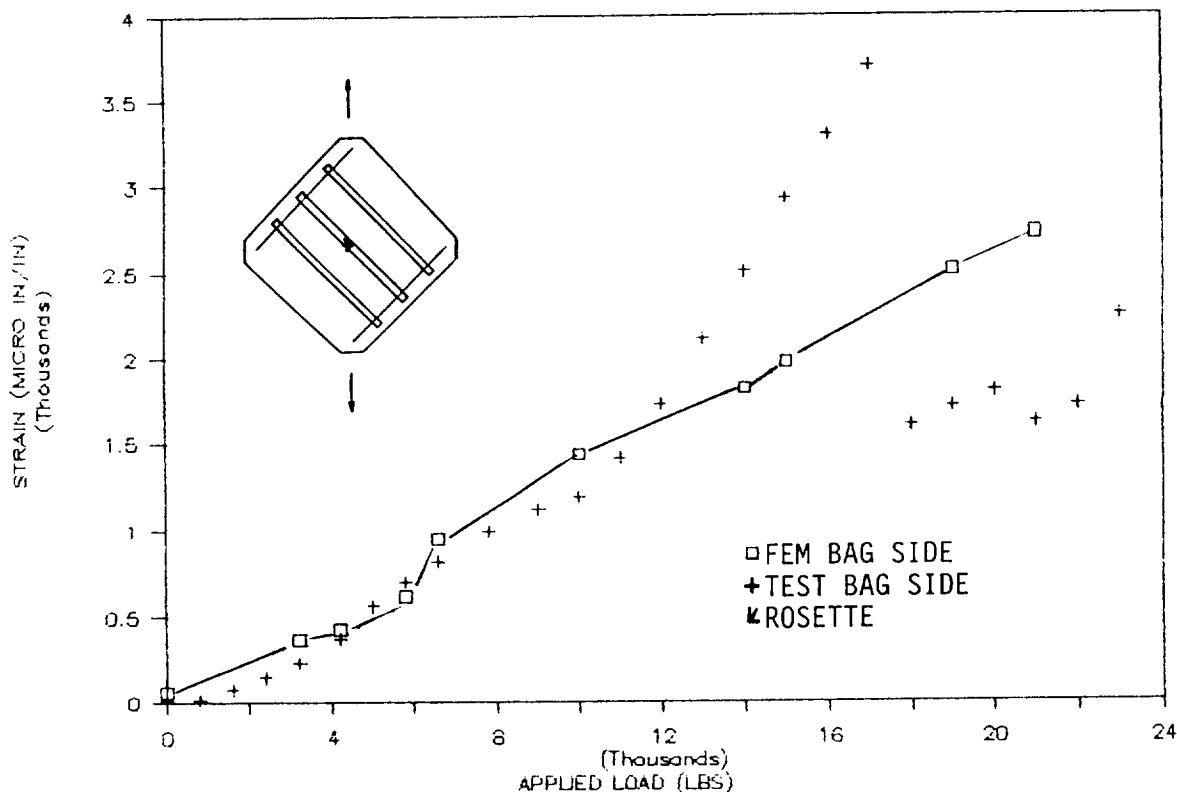
226

Figure 22. Comparison of Finite Element Predictions to Test Results
at Hat-Stiffener Center (Shear Strains - Full Scale Panel)

detailed finite element analysis (up to buckling) with the same mesh but with smaller load increments showed the predicted bifurcation load to be 102 lb/in or 8% higher than the bifurcation load indicated by the deflection gage during test. It was a snap-through buckling where the skin, up to that point deflecting in the direction of the panel curvature, reversed direction with a jump in deflection of more than an order of magnitude. The average failure load of 23500 lbs (554 lbs/in) gives a postbuckling factor (failure load to buckling load ratio) of 5.9.

The failure progression as observed during test and inferred from examination of failed specimens was as follows: (1) Upon loading to 18000-19000 lbs, fiber cracking and matrix splitting were observed at one of the loaded corners of the specimen (see Figure 26 point O). This is consistent with the starting crack observed during testing of the flat frame-stiffener intersection specimen and is at approximately the same location. Like the flat frame/stiffener intersection specimen, the crack on the full-scale article stopped after growing to a size of 3-4 inches. It is believed this crack initiated as a result of the test fixture pinching the lower corner of the specimen and served as a stress relief mechanism. The conjecture that this crack did not cause final failure was verified by the fact that each test specimen failed at significantly higher load, 4000-5000 lbs after the corner crack developed.

At 23000 to 24000 lbs of applied load, new fiber and matrix cracks were noted to initiate as a result of large displacement gradients caused by the buckled shape at the frame and hat stiffener intersection (see point F in Figure 26). These cracks, accompanied by some delamination, progressed from the
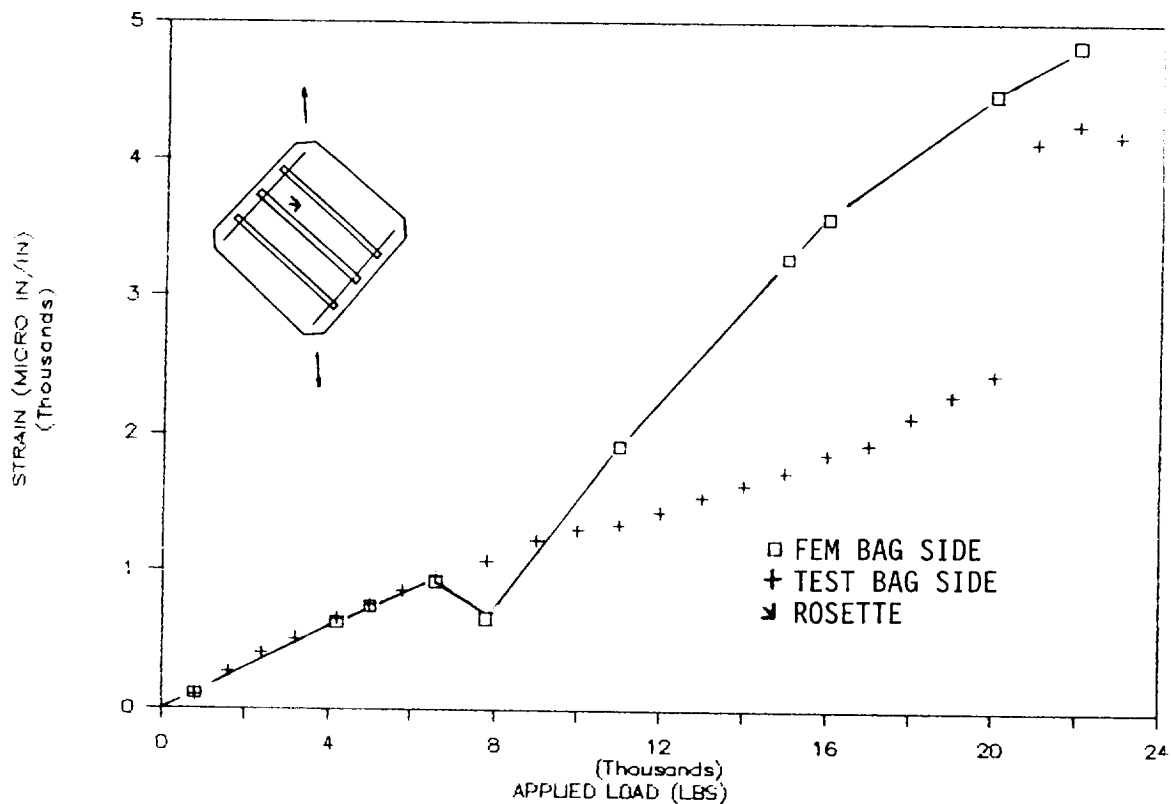
227

Figure 23. Comparison of Finite Element Predictions to Test Results
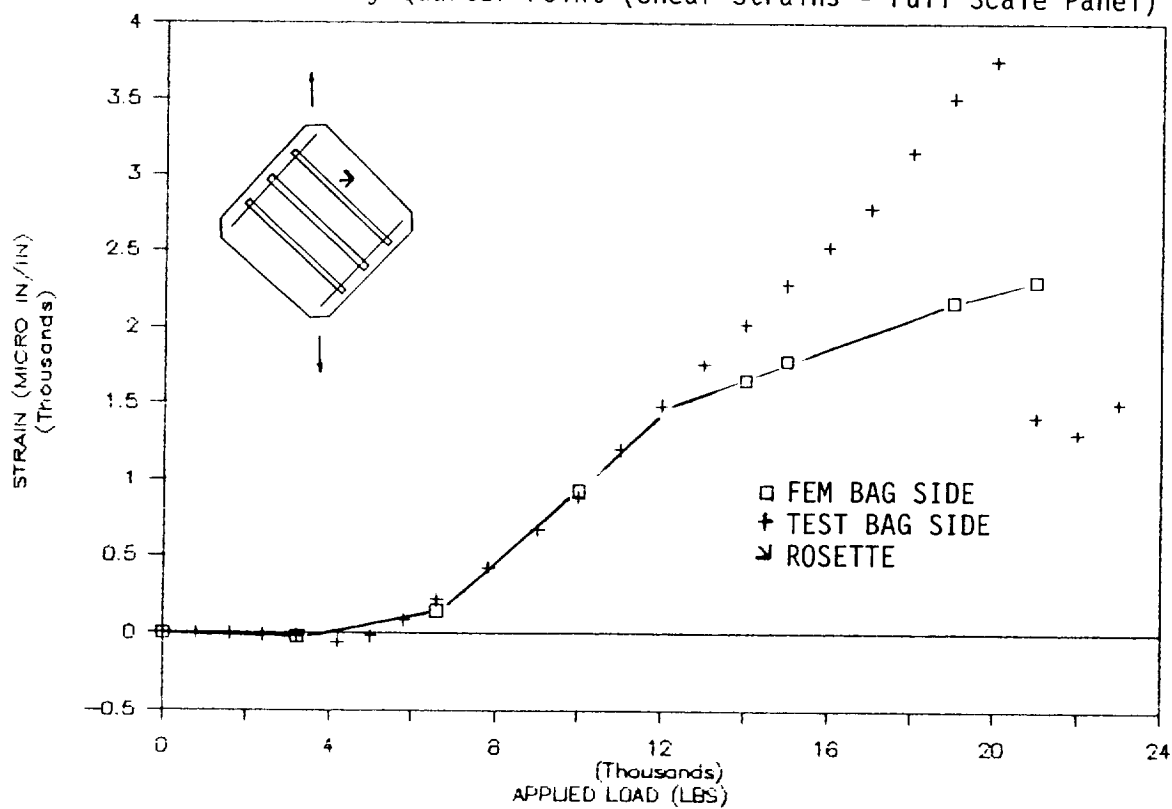at Bay Quarter Point (Shear Strains - Full Scale Panel)



Figure 24. Comparison of Finite Element Predictions to Test Results
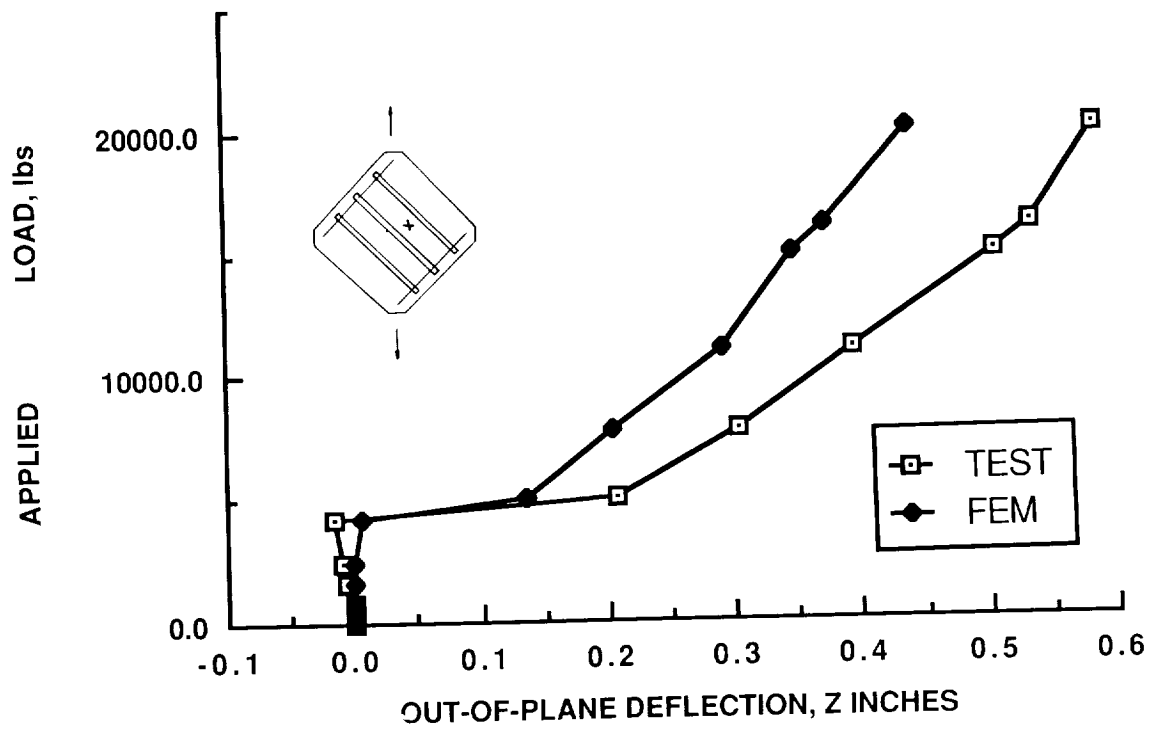at Bay Center (Shear along Frame Axis - Full Scale Panel)

228

Figure 25.  Load versus Deflection Plot at Bay Center (Finite Element
Prediction and Test Measurement)

intersection along the edge of one of the hat stiffeners, propagated across the hat stiffener, and continued to final failure as marked by separation of the specimen into two large sections. The resulting fracture pattern is also shown in Figure 26. It should be noted that the flanges of the frames and stiffeners were embedded in the skin and no stiffener separation from the skin was noted. This is different from the common failure of these panels when the flanges are bonded directly on the skin (see for example reference 8) and shows that this configuration is effective in altering and delaying stiffener-to-skin failures in such panels.

Failure of the full-scale panels is predicted using the results of the flat frame-stiffener intersection specimens which showed very similar failure mode. As is shown in Figure 27, the shear strains at the bay center for the two specimens are very close to each other up to a load of 12000 lbs. At that point, the full-scale panel diverges probably due to a change in the mode shape that essentially reversed the buckling pattern. It is believed that the strains at the location where final failure started for both flat and curved specimens are similar and thus the loads (in lbs/in of shear) at which internal strains reach the material allowables should be the same for both types of specimen. The failure load for the flat specimen then should be a reasonable approximation to the full-scale article failure load. As already mentioned, the failure load for the full-scale article was 554 lbs/in which is 11% lower than the value of 614 lbs/in that the flat specimen failure would predict.

## SUMMARY AND CONCLUSIONS

A program is on-going to evaluate the structural performance of composite fuselage structure fabricated using an autoclave THERM-X$^{sm}$ process. A building block approach is used to isolate failure modes and quantify load paths and failure loads for the full-scale article which is a curved skin panel with cocured hat stiffeners and frames with a tee-shaped cross section. Tests at the coupon and element level have shown that the THERM-X$^{sm}$ processed parts have comparable stiffness, strength, and failure modes. The only instant where the THERM-X$^{sm}$ processed parts showed moderate inferiority (up to 15%) to conventionally manufactured parts was in high speed-low impactor mass compression after impact test.

Finite element predictions of deflection shape and strains in the flat element level tests are in good agreement with test results except at some locations in the panel where at intermediate loads the test results suggest a difference in the postbuckled deflection shape.

The curved stiffened panel performed very well, exceeding the design ultimate load of 250 lbs/in by over a factor of 2 and failing at a postbuckling factor of 5.9. The finite element predictions are in good agreement with the test results up to a postbuckling factor of 3. At higher loads the test results suggest that local failures and changes in mode shapes took place that were not accounted for by the finite element analysis. The failure mode involved cracks starting at a frame stiffener intersection but no flange separations were noted (due to the use of embedded flanges) nor any shear tie failures. This suggests that failure is driven by in-plane skin failure in the vicinity of frame/ stiffener intersections where stress concentrations will be present. More work is needed to better quantify this failure mode.
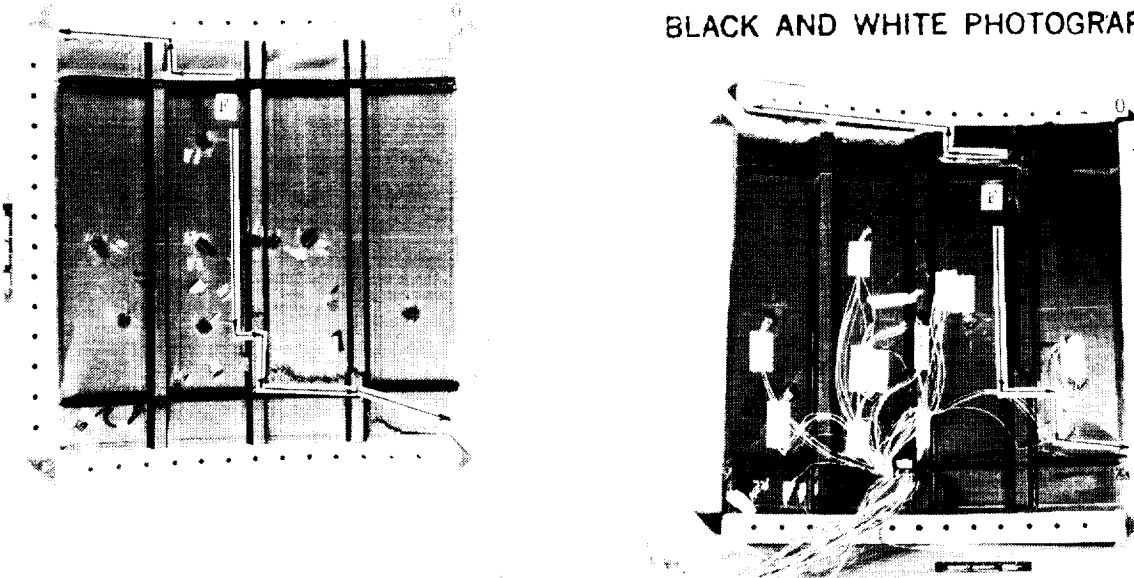
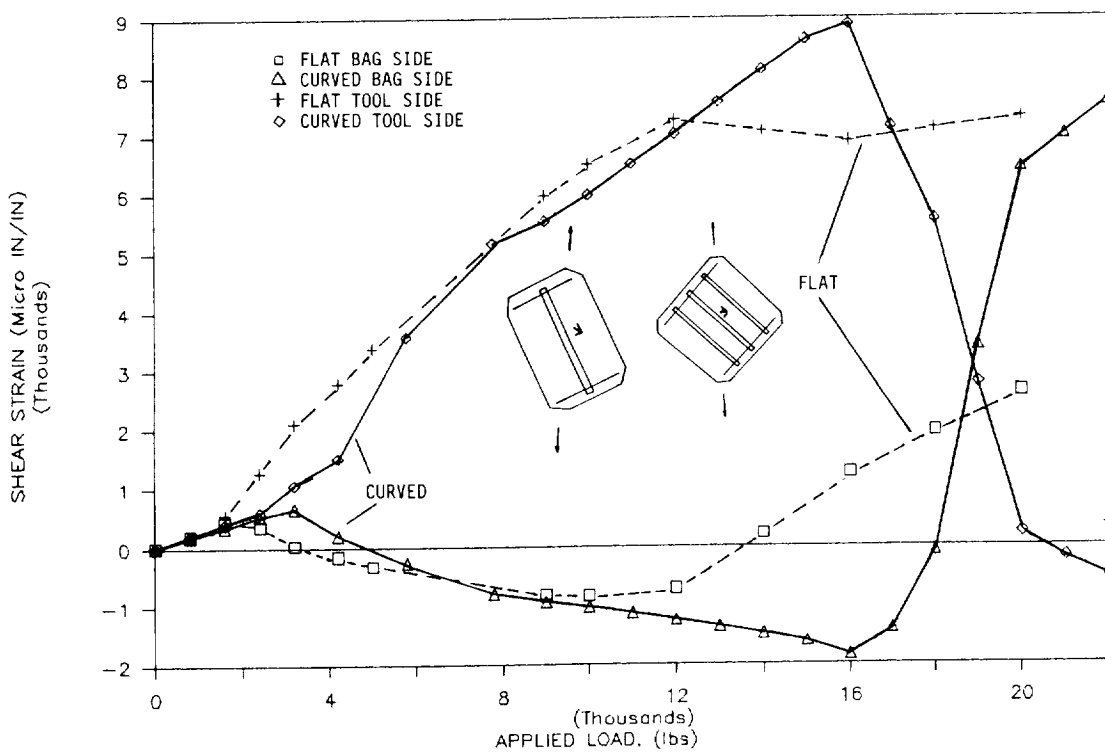Figure 26. Failure Mode for First Two Full-Scale Tests



Figure 27. Shear Strain Comparison for Intersection and Full-Scale
Tests (Bay Center)

Failure predictions for the curved panel can be obtained using the failure load from the flat element level test which had a similar failure mode. That prediction is 11% higher than the curved panel failure load.

The fact that the finite element analysis assuming the THERM-X$^{sm}$ processed parts had the same properties as conventionally manufactured parts showed good agreement with test results up to the point where local failures and mode changes not accounted for in the finite element analysis became significant, suggests that undamaged THERM-X$^{sm}$ processed parts are structurally equivalent to conventionally manufactured parts.

THERM-X$^{sm}$ processing enables manufacture of high quality complex parts with corners and tight radii with minimum tooling and at low cost.

## ACKNOWLEDGMENT

## REFERENCES

1. Kassapoglou, C.; DiNicola, A.J.; and Chou, J.C.: Structural Evaluation of Composite Fuselage Structure Fabricated Using a THERM-X$^{sm}$ Process. Proceedings of 46th American Helicopter Society Forum, Washington DC, 1990, pp. 671-682.

2. Boeing Structural Test Components Presentation, Workshop on Common Structural Test Components for ACT, Newport News, May 1990.

3. Cantwell, W.J.; and Morton, J.: The Influence of Varying Projectile Mass on the Impact Response of CFRP. Composite Structures, vol 13, 1989, pp. 101-114.

4. Cantwell, W.J.; and Morton, J.: An Assessment of the Residual Strength of an Impact Damaged Carbon Fibre Reinforced Epoxy. Composite Structures, vol 14, 1990, pp. 303-317.

5. Error Due to Transverse Sensitivity in Strain Gages, M-M Technical Note TN-509, Micro Measurements Division, Measurement Group, Inc, Raleigh, NC,1982.

6. Dally, J.W.; and Riley, W.F.: Experimental Stress Analysis, McGraw Hill, Inc, 1978, chapters 12.5 and 12.6.

7. Tsai, S.W.: Strength Characteristics of Composite Materials. NASA OR-224, April 1965.

8. Rouse, M.: Postbuckling and Failure Characteristics of Stiffened Graphite-Epoxy Shear Webs. 28th SDM Conference, Monterey CA, April 1987, AIAA paper 87-0733.